Validation of DEM modeling of sintering using an in situ X-ray microtomography analysis of the sintering of NaCl powder

Sylvain Martin, Sebastián Navarro, Hervé Palancher, Anne Bonnin, Jacques Léchelle, Mohamed Guessasma, Jérôme Fortin, Khashayar Saleh

Validation of DEM modeling of sintering using an *in situ* X-ray microtomography analysis of the sintering of NaCl powder

Sylvain Martin[1], Sebastian Navarro [2], Hervé Palancher [3], Anne Bonnin [4], Jacques Lechelle[3], Mohamed Guessasma[5], Jérôme Fortin[5], and Khashayar Saleh[2]

[1] École des Mines de Saint Etienne, LGF UMR 5307, 158 Cours Fauriel, 42023 Saint-Etienne Cedex 2, France
[2] Université de Technologie de Compiègne , EA 4297, TIMR, France
[3]CEA DEN, CAD, DEC, SESC, LLCC , 13108 Saint Paul lez Durance, France
[4]Paul Scherrer Institut , Swiss Light Source, Villigen, Switzerland
[5]Université de Picardie Jules Verne , EA 3899, LTI, France

August 2015

Abstract

This paper aims to validate the Discrete Element Method (DEM) model of sintering. *In situ* X-ray microtomography experiments have been carried out at the ESRF to follow the sintering of $NaCl$ powder, the properties of which are close to the DEM model assumptions.

DEM simulations are then run using an improved implicit method. The comparison between experiment and simulation shows the capability of DEM to predict the behavior of the sample on both particle and packing scale.

The main advantages and limits of this approach are finally discussed based on these results and those of previous studies.

1 Introduction

For the last years, *in situ* X-ray microtomography has become a common approach to monitor the microstructure parameters during sintering [1, 2, 3]. The individual behavior of every pair of particles in contact can indeed be followed during the sintering process thanks to this method. Thus, it allows very useful

comparisons between the average behavior of particles in contact within the packing and macroscopic parameters [4]. This method was also used to investigate the capability of different numerical approaches to get a realistic representation of the microstructure evolution, like Monte Carlo [5, 6] and DEM simulations [4]. The latter study showed that DEM modeling matched well experimental data in terms of relative motion of particles but not with respect to time. The copper powder used was indeed polycrystalline which is not taken into account in DEM simulations.

In this paper, we tried to validate the capability of DEM simulation to predict the motion of particles during sintering in the simplest case, that is to say a powder whose properties are consistent with DEM assumptions. Hence, it was decided to investigate the sintering of $NaCl$ powder which is composed of monocrystal and whose thermodynamic and kinetic properties are well known in the literature [7]. The *in situ* synchrotron X-ray microtomography experiments were performed at the *ESRF* of Grenoble.

The DEM simulations were run using an original implicit approach based on *Non Smooth Contact Dynamics* [8] that allows the avoidance of mass scaling. The authors showed in previous study that this method leads to a better representation of rearrangement during sintering [9].

2 Experiments

The aim of the experiments was to get accurate data on the kinetics of early stage sintering in order to validate the DEM model. Hence, the experimental powder was expected to be close to DEM model assumptions. $NaCl$ powder was found to be a relevant choice according to the following criteria:

- most of commercial $NaCl$ powders are monocrystalline,
- thermodynamic and kinetic properties are well known in the literature,
- grain boundary diffusion is predominant at low temperature,
- One can show that the polyhedral shape of $NaCl$ particles does not have much influence on the kinetics of sintering [7],

The sample holder was a 3 mm high cylinder with a diameter of 1 mm, which led to a voxel edge of 1.3 μm to get the full sample on the tomography images.

Thus, a commercial $NaCl$ powder was chosen according to its granular size distribution. It was then sieved at 100 μm which was found to be the best compromise according to the size of the sample holder, the kinetics of sintering and the voxel edge.

This monocrystalline property was verified for the selected powder by an EBSD analysis that was carried out on a few particles. An example of the results is given in Figure 1. It shows that the cystallographic orientation is constant over the upper face of the particle, which proves that the particle is a

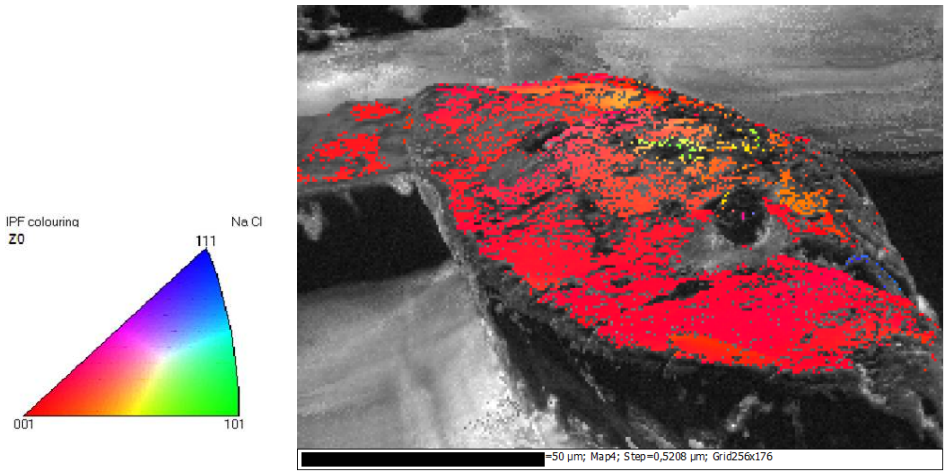

a b

Figure 1: EBSD analysis of a particle of $NaCl$, crystal orientation corresponding to the color range (a) and image of the $NaCl$ crystal (b)

monocrystal. It should be noticed that many areas remain grey on the picture. It comes from surface roughness since the materials was not polished. Roughness stops a part of the back-scattered electrons which prevent the orientation from being analyzed. However, those grey areas are not wide enough to generate uncertainty on the homogeneity of the face orientation.

The DEM model is well suited for the representation of the early stage of densification due to grain boundary diffusion. Hence, the experimental conditions were chosen to increase grain boundary diffusion and reduce the effect of other phenomena like gas transport.

The map of predominance of the different diffusion path, which is given in [7], shows that for particles of 100 μm, grain boundary diffusion dominates at low temperature and gas transport becomes dominant close to the melting temperature. Moreover, the air pressure (1 atm) allows a reduction of gas transport. It should be noticed that dominant gas transport would have led to an increase of the neck radii, i.e. solidification, without densification. Hence, the sample was sintered at 973 K under 1 atm of air during 500 min.

During the experiment, microtomography were run *in situ* every 40 min. The acquisition time is about 30 min. It means that the microstructure might have changed slightly during the first tomography, but according to the quality of the images, it appears that this evolution remains reasonable.

Figure 2 represents clipping plans of the $3D$ images at different stages of the experiment. It appears that the phase contrast imaging lead to a clear segmentation of solid and gas phase.

The 3D images were then analysed using *Imorph* [10]. This piece of software carries out the segmentation of particles and contact detection. An example of

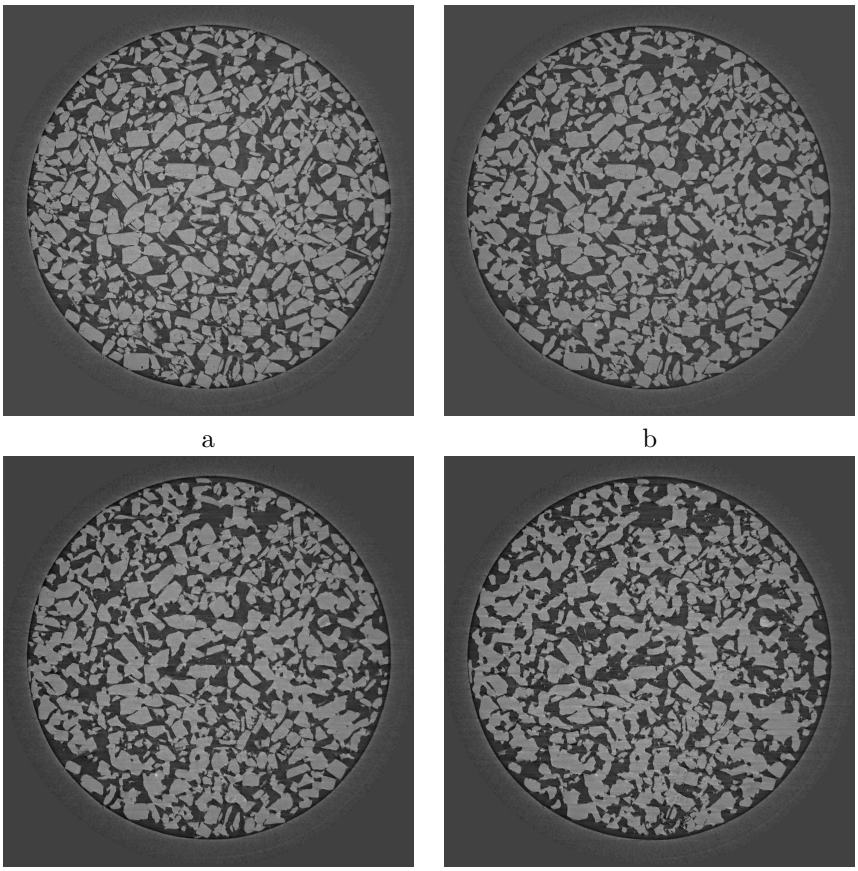

Figure 2: Microtomography clipping plan of the $NaCl$ sample after 0 min (a), 135 min (b), 256 min (c) et 500 min (d) of sintering at 973 K

$3D$ images after particles segmentation is given in Figure 3. It can be observed that most of particles are well defined, but some of them are splitted into two or more particles.

The segmentation step requires indeed that the borders of particles be visible. Hence, this operation becomes more and more complicated when the contact network is getting denser.

The settings that have to be determined from the tomography images can be classified in three categories :

- Parameters that represent the macroscopic behavior of the packing, like density. They only require a contrast between the gas and solid phase. Thus, density has been measured over the all experiment.

- Average characteristics of the behavior of particles, like coordination num-

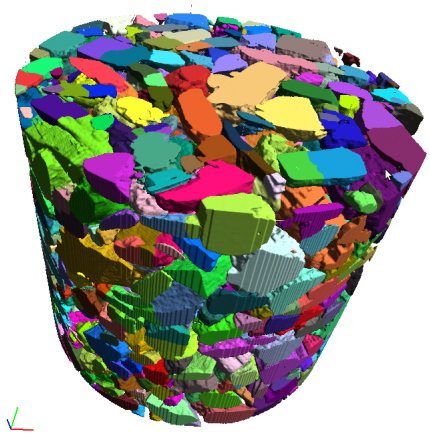

Figure 3: 3D segmentation of particles obtained from reconstruction of a microtomography image

ber. The latter needs an individual segmentation of particles on the tomography images. However, even if some particles are split into two or more parts during the segementation step, the average value would be only slightly modified. In other words, particles do not need to be identified individually on the successive tomography images. Hence, this criteria was also measured throughout the 500 min.

- Settings of the behavior of individual particles in contact, like center to center approach of particles in contact or rearrangement parameters. These criteria require an individual identification of every particle over the different images. Particles and contacts can be lost very easily if the segmentation is not perfect. In this way, after 250 min, the necks of particles in contact are too big to allow a proper detection of individual particle borders. Thus, these parameters were only measured on the eight first pictures.

3 DEM simulation

3.1 Sintering model

The principle of the DEM approach is to consider a packing in which individual particles interact through a contact law. Thus, it is based on strong assumptions which allow the representation of particle-particle interactions using simple analytical laws.

In this study, the numerical method is an original implicit DEM which is slightly different from the traditional explicit DEM used by [11] and [12]. The simulation of sintering using an explicit method requires indeed a dramatic

increase of the mass of particles (i. e. mass scaling), due to the very small critical time step. This issue has been discussed in the literature and first improvements were proposed by Nosewicz et al. [13] to reduce the dependance to mass scaling.

To overcome this issue, an implicit method based on the Non Smooth Discrete Element Method was adapted to the sintering model by the authors. Thus, we showed that avoiding mass scaling led to a more realistic representation of rearrangement [9]. The description of this improved numerical method is out of the scop of this paper, but further information is available in [14, 9]. Since the sintering model and optimized DEM algorithm are fully described in the references above, only the main aspects of the model will be given here.

The main assumptions associated with the model are as follows :

- Particles are and remain spherical over the simulation.
- Grain boundary is represented by a disk and the dihedral angle remains constant.
- Densification is due to grain boundary diffusion which take matter out of the contact area.
- Fast surface diffusion assumption is used. It means that surface diffusion lays out, along the free surface, the matter which has been brought at the surface of the neck by grain boundary diffusion. However, the contribution of surface diffusion to the growth of the neck is not considered.

The contact law is composed of a normal force and a tangential resistance to sliding force. The normal force can be written as follows :

$$f_n = -\frac{\alpha}{\beta}\pi R\gamma_s + \frac{\pi r^4}{2\beta\Delta_b}V_n \tag{1}$$

where r is the neck radius which vary as $\frac{dr}{dt} = \frac{R}{r}\ V_n$, γ_s is the surface energy, V_n is the center to center approach velocity and Δ_b can be written $\Delta_b = \frac{\Omega\delta_b D_b}{kT}$ with Ω the atomic volume, D_b the coefficient for grain boundary diffusion and δ_b its thickness. α and β are functions of the ratio of grain boundary and surface diffusion [15] which are taken as follows : $\alpha = 9/4$ and $\beta = 4$. R is the equivalent radius of particles defined as $R = 2 \times R_1R_2/(R_1 + R_2)$.

The tangential force is given in Equation 2:

$$f_t = -\eta\frac{\pi r^2 R^2}{2\beta\Delta_b}\dot{u}_t \tag{2}$$

with $\dot{u}_t$ the sliding velocity along the grain boundary and η a dimensionless coefficient that was taken equal to 10^{-3} according to Martin and Bordia [16].

Simulations were run using the DEM software *MULTICOR*, which is developed at the Université de Picardie Jules Verne [17].

3.2 Simulation parameters

To get a realistic simualtion of sintering, it is necessary to bring the initial properties as close as possible to the experiments. For example, it was shown by Rasp et al. [18] that a higher initial coordination number with unchanged initial density leads to faster densification rate.

The main properties of the initial packing are the Particle Size Distribution (PSD), the relative density D and the coordination number Z (i.e. the number of contacts per particle).

The PSD of the $NaCl$ powder was determined using a morpho-granulometric analysis and was then used to generate the numerical powder. Then, the packing density, the pore size distribution and the initial coordination number were extracted from the analysis of the microtomography image.The PSD and pore size distribution are given in Figure 4.

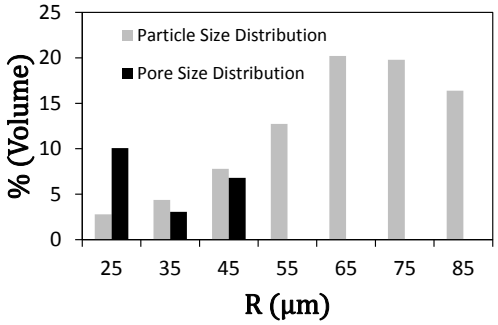

Figure 4: Initial Particle and Pore Size Distribution of the $NaCl$ powder

To make the initial packing according to the required properties, a random cloud of particles was generated using experimental PSD and density and was then followed by a deposition DEM simulation. The simulation stopped when the global kinetic energy reached zero, which means that the packing was at the equilibrium.

This procedure allows to control the coordination number by adjusting the DEM parameter like the particle cohesion or the weight of the gravitation force during the deposition process. The control of the pore size distribution is more complicated. Thus, a procedure proposed by Olmos [19] was implemented, which consists in adding extra particles in the intial packing, the PSD of which mach the pore size distribution of the experimental sample. Those particles are then removed between the sintering simulation.

The initial numerical particle packing was generated using an open source DEM software *LIGGGHTS* [20]. The full procedure can be summed up as follows:

- First of all, a random cloud of particles is created according to the given density, PSD and including extra particles corresponding to the pore size

	$D^o(\%)$	Z
Exp	55.6	5.
DEM	55.6	4.

Table 1: Initial properties of experimental and numerical assemblies

distribution.

- Then, a simple DEM calculation is run. Particles start to move due to the repulsive force produced by overlapping particles. Kinetic energy is then dissipated through collisions until the system tends toward equilibrium.
- When the kinetic energy of the system becomes close to 0, the calculation is stopped.
- Then the extra particles (which represent pores) are removed from the assembly. The initial packing is now ready.
- Finally the results files are red by MULTICOR and used to define the initial packing for the sintering simulation.

Density and coordination number for the experimental and numerical initial sphere packing are given in Table 1.

It should be noticed that the coordination number remains slightly lower in the numerical packing. Insofar as it was not possible to reach the exact values for both density and coordination number, simulation of sintering were run for a few assemblies with slight variations of initial properties. It was found that those variations dragged very slights differences in values for the targeted parameters but no change for the tendencies neither for the shape of the curves of those parameters. It can be explained by the fact that our simulations focus only on the very early stage of sintering.

The thermodynamic and kinetic properties of $NaCl$ powder were taken from [7] and are given in Table 2. It should be noticed that all parameters are taken from the literature which means that there is no fitting parameter in the simulation.

$\delta(m)$	$D_b(m^3/s)$	$\Omega(m^3)$	$\gamma_s(J/m^2)$
7.98×10^{-10}	3.7×10^{-9}	4.49×10^{-29}	0.28

Table 2: Properties of $NaCl$ powder [7] at 973 K

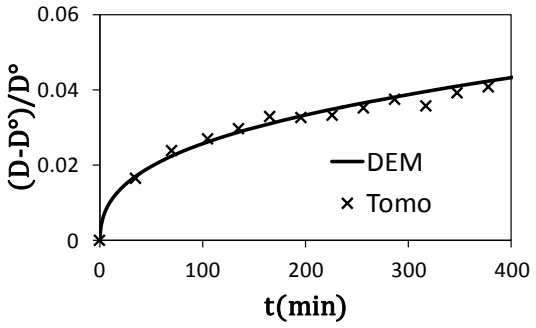

Figure 5: Evolution of relative density during sintering of $NaCl$ powder at 973^oK, with D and D^o respectively the density and initial density. Experiment (Tomo) and simulation (DEM) results.

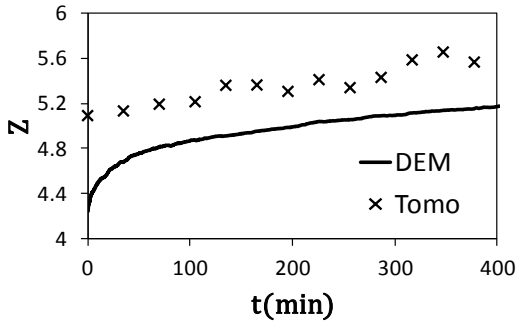

Figure 6: Evolution of coordination number Z during sintering of $NaCl$ powder at 973^oK, experiment (Tomo) and simulation (DEM) results

4 Results and discussion

4.1 Results

On the sample scale, the density D and average coordination number Z are the most relevant parameters. The results for both DEM simulation and experiment are given in Figure 5 and Figure 6.

Then, relative neck radius r/R and relative indentation h/d can be used to characterize the kinetics of sintering of particles in contact within the sample. In order to compare numerical and experimental results, it was chosen to use the relative indentation which is easier to measure on the tomography images. Indentation corresponds to center to center approach of particles in contact h, as shown in Figure 7 and is then normalised by the initial distance between particles when contact is punctual: $d = R_1 + R_2$.

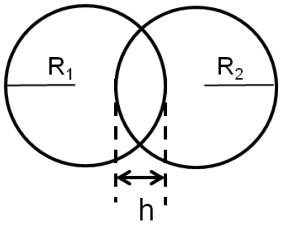

Figure 7: Definition of indentation h for two particles in contact

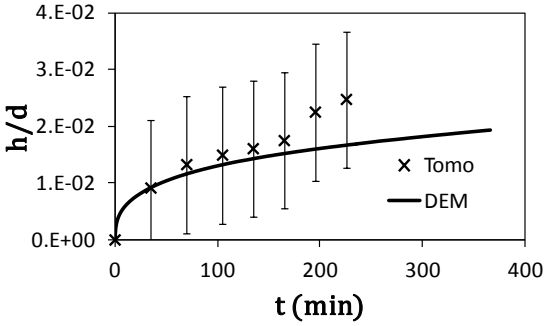

Figure 8: Evolution of relative indentation h/d during sintering of $NaCl$ powder at 973 K, with h the indentation parameter and $d = R_1 + R_2$. Experiment (Tomo) and simulation (DEM) results

For the experimental powder, d is defined as the distance between the center of mass of particles in contact on the first tomography image. Then, h at a time t is can be calculated as $h = d - d(t)$, with $d(t)$ the distance between the center of mass of the same particles in contact measured on the image which correspond to time t.

Because of the complexity of segmentation and identification of individual particles over the experiment, only 30 pairs of particles in contact were identified in the 8 first images. Moreover, the order of magnitude of h is the same as the voxel edge. This leads to very high uncertainty on the experimental measurement of h/d. The results for indentation are plotted in Figure 8.

Finally, the individual motion of particles can be characterized by the rearrangement angle θ. The latter, defined by [4], represents the angle between the theoretical direction of particles displacement and the real motion of particles. According to the mean field assumption, the *theoretical* displacement is directed toward the center of the assembly. Reciprocally, the center of the assembly can be defined as the geometrical point which corresponds to the mean direction of the particles. Hence, this geometrical point has to be determined properly to calculate θ. Its theoretical location is at the middle of the horizontal plan and at

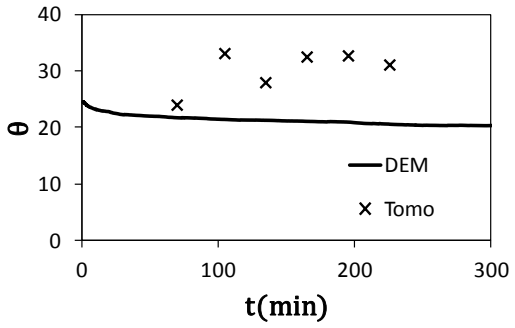

Figure 9: Evolution of rearrangement parameter θ during sintering of $NaCl$ powder at 973 K. Experiment (Tomo) and simulation (DEM) results

the bottom on the vertical axis. However, the sample holder is slightly conical and the tomography analyses show that the powder pellet moved slightly toward the top during the experiment. Thus, the experimental *center* was determined as the geometrical point which maximizes the reduction of the distance between this point and the particles during the sintering process. Then, θ was mesured following the individual motion of particles through the different images. The results are given in Figure 9.

4.2 Discussion

The aim of this work was to evaluate the capability of the DEM simulation to predict the evolution of the main microstructure parameters versus time. Hence, it was necessary to adapt the operating conditions to the model assumptions. At 973 K and under atmospheric pressure, grain boundary diffusion is predominant and the kinetics of sintering between two particles can be modelled by Equation 1. However, the choice of a relatively low temperature lead to a slow evolution of the microstructure. Moreover, the particle segmentation issue of the tomography images prevented the analysis of the full tomography data. Thus, our results concern only the very earlier stages of sintering which explains the low value of the final coordination number, density and indentation.

Despite the small number of contacts that were followed on the tomography images, Figure 8 shows that the evolution of the average center to center approach between particles in contact is very satisfying. It also means that the polyhedral shape of $NaCl$ crystals does not have much influence on the kinetics of indentation, which is in good agreement with Goodall et al. [7]. The simulation results are also very close to the experiments for the density evolution, which shows a good capability of DEM to simulate the scaling up between the contact interactions and the macroscopic behavior of the sample.

The coordination number plays a major role in the densification process.

The apparition of new contacts with higher kinetics enhance rearrangement and, thus, speeds up densification. The initial coordination number was lower in the simulation than in the experiment, due to the polyhedral shape of $NaCl$ crystals. However, both curves are almost linear with an identical slope.

In the first stages of sintering, rearrangement is also responsible for contact opening, changes in the angles between the lines connecting the center and of particles and, more generally speaking, evolutions of the packing structure Exner and Mller [21].

In this study, we chose to measure rearrangement using the parameter θ proposed by Olmos et al. [4]. Figure 9 shows that the order of magnitude of this parameter is similar in the simulation and in the experimental sample, although it seems slightly underestimated by the simulation. However, it is very tricky to go further in the analysis. The poor accuracy of the estimation of the geometrical center of the sample, which is used in the experimental calculation of θ, does not allow any conclusion based on this small difference. Moreover, the deviation of θ can be high between different particles, which means that it should be averaged over many more particles to get a smooth curve. This is why the experimental values are very dispersed.

4.2.1 DEM and sintering

The main advantage of the DEM approach is to consider individual interactions between particles in contact, which allows a more complete description of the microstructure evolution than the mean field models. The interest of DEM increases with the width of the the polydispersity which is the main parameter responsible for rearrangement [22]. Here, the PSD has one single peak with a size ratio limited to $1:4$ and both initial density and coordination number are too low to enhance rearrangement and densification. Thus, the experimental configuration is not well designed to focus on the role of the local contact network on the microstructure evolution but this point has already been investigated in previous works [4]. On the other hand, our results show that, in a simple case with experimental conditions close to the model assumptions, the DEM approach is able to predict the microstructure evolution for the early stage of sintering on contact and sample scale.

The model for two particles in contact given by Equation 1 and Equation 2 allows only one degree of freedom for the geometrical evolution of particle which is the center to center approach. Nevertheless, the ratio of surface and grain boundary diffusion can be taken into account using different values of α and β in Equation 1, [15]. It could also be possible to estimate the values of these coefficients in the case of domination of coupled grain boundary and gas transport phenomena. The latter plays indeed the same role as surface diffusion. On the other hand, introducing the contribution of surface diffusion or gas transport to the neck growth would require to redefine the geometrical model [23] to ensure mass conservation.

The particle morphology has not been investigated so far by the DEM approach. The spherical particle assumption is indeed used in all the simulations

of sintering based on DEM approaches. Even if it appears that the polyhedral shape of $NaCl$ does not have much influence on the sintering kinetics in the early stage, it clearly changes the local structure of the packing. The most visible effect is the coupled value of density and coordination number that could not be reached using our spherical numerical particles. A polyhedral shape is also expected to change the ability of particles to slide or rotate compared to spherical ones. In the case of sintering, monocrystalline particles remains non spherical because of surface energy anisotropy. This anisotropy is a function of crystal orientation. Thus, crystal morphology at equilibrium can be predicted using Wulff diagram [24]. The introduction of non spherical particles in the simulation would be critical in terms of calculation time but would give relevant information about contact network and structure that is not available so far. A first step could be to modify slightly the geometrical model to introduce non spherical particles but without considering anisotropy of surface and grain boundary energies.

Finally, the main limits of the DEM approach is to consider only the center to center approach of particles, neglecting major phenomena that appear in later stages like grain growth. DEM only represents the motion of particles within the packing, while later stages of sintering are dominated by interface motion which is responsible for grain growth. These phenomena are well modelled by specific numerical methods like phase field [25].

The next challenge for the DEM simulations is to be able to represent both particles and grain boundary motion, or at least to consider a simple model for grain growth. DEM approach could be improved by introducing a simple law which gives mass transfer across grain boundary for two particles in contact with respect to particle size ratio and neck radius and using this law to update the size of particles with respect to time. The development of this model requires accurate information about two particles in contact. The more complete approach on a particle scale is given by the mechanical approach which is very promissing but not working yet [26, 14]. Further works on these models might allow the development of such laws for introducing grain growth in DEM.

It should also be noticed that recent works aim at unifying phase field and DEM [27]. Those target at simulating sintering for early and advanced stages of sintering with a single calculation, but the simulations are limited so far to a very low number of particles.

5 Conclusion

This study shows the capability of DEM approach to predict the microstructure evolution in a simple case with operating conditions adapted to match the model assumptions. Those assumptions are the main limit of DEM simulation of sintering. However, DEM remains the only numerical approach which allows the representation of the individual motion of particles within the packing, taking into account the competition between neighbouring contacts interactions and then forces network. Thus, DEM is relevant for the simulation of early stages

of sintering where the predominant phenomena match the physical and geometrical assumptions of the model. Moreover, only a few studies have investigated the application of DEM to sintering so far. Further work should allow to bring forward the capability of this approach, introducing new phenomena like grain growth in the DEM model of sintering.

Acknowledgement

Many thanks to Xavière Iltis from the CEA/DEN/CAD/DEC/SFER/LCU for the EBSD analysis

References

[1] O. Lame, D. Bellet, M. Michiel, D. Bouvard, In situ microtomography investigation of metal powder compacts during sintering, Nuclear Instruments and Methods in Physics Research Section B: Beam Interactions with Materials and Atoms 200 (2003) 287 – 294. Proceedings of the E-MRS 2002 Symposium I on Synchrotron Radiation and Materials Science.

[2] O. Lame, D. Bellet, M. Di Michiel, D. Bouvard, Bulk observation of metal powder sintering by x-ray synchrotron, Acta Materialia 52 (2004) 977984.

[3] A. Vagnon, O. Lame, D. Bouvard, M. D. Michiel, D. Bellet, G. Kapelski, Deformation of steel powder compacts during sintering: Correlation between macroscopic measurement and in situ microtomography analysis, Acta Materialia 54 (2006) 513 – 522.

[4] L. Olmos, C. L. Martin, D. Bouvard, D. Bellet, M. Di Michiel, Investigation of the sintering of heterogeneous powder systems by synchrotron microtomography and discrete element simulation, Journal of the American Ceramic Society 92 (2009) 14921499.

[5] S. Bordre, D. Bernard, D. Gendron, J.-M. Heintz, Characterisation of elementary sintering processes using monte carlo simulation and x-ray computed microtomography, Computational Methods in Materials Characterisation 6 (2003).

[6] C. G. Cardona, V. Tikare, B. R. Patterson, E. Olevsky, On sintering stress in complex powder compacts, Journal of the American Ceramic Society 95 (2012) 2372–2382.

[7] R. Goodall, J.-F. Despois, A. Mortensen, Sintering of nacl powder: Mechanisms and first stage kinetics, Journal of the European Ceramic Society 26 (2006) 3487 – 3497.

[8] J. J. Moreau, Some numerical methods in multibody dynamics: application to granular materials, European journal of mechanics. A. Solids 13 (1994) 93114.

[9] S. Martin, M. Guessasma, J. Léchelle, J. Fortin, K. Saleh, F. Adenot, Simulation of sintering using a non smooth discrete element method. application to the study of rearrangement, Computational Materials Science 84 (2014) 31 – 39.

[10] E. Brun, De l'imagerie 3D des structures l'étude des mécanismes de transport en milieux cellulaires, Ph.D. thesis, Université de Provence, 2009.

[11] B. Henrich, A. Wonisch, T. Kraft, M. Moseler, H. Riedel, Simulations of the influence of rearrangement during sintering, Acta Materialia 55 (2007) 753762.

[12] C. L. Martin, H. Camacho-Montes, L. Olmos, D. Bouvard, R. K. Bordia, Evolution of defects during sintering: Discrete element simulations, Journal of the American Ceramic Society 92 (2009) 14351441.

[13] S. Nosewicz, J. Rojek, K. Pietrzak, M. Chmielewski, Viscoelastic discrete element model of powder sintering, Powder Technology 246 (2013) 157–168.

[14] S. Martin, Contribution à la modélisation du frittage en phase solide, Ph.D. thesis, Compiègne, 2014.

[15] D. Bouvard, R. M. McMeeking, Deformation of interparticle necks by diffusion-controlled creep, Journal of the American Ceramic Society 79 (1996) 666672.

[16] C. Martin, R. Bordia, The effect of a substrate on the sintering of constrained films, Acta Materialia 57 (2009) 549558.

[17] E. Sanni, I.and Bellenger, J. Fortin, P. Coorevits, A reliable algorithm to solve 3D frictional multi-contact problems: Application to granular media, Proceedings of the Thirteenth International Congress on Computational and Applied Mathematics (ICCAM-2008), Ghent, Belgium, 711 July, 2008 234 (2010) 1161–1171.

[18] T. Rasp, T. Kraft, H. Riedel, Discrete element study on the influence of initial coordination numbers on the sintering behaviour, Scripta Materialia (2013).

[19] L. Olmos, Etude du frittage de poudres par microtomographie in situ et modlisation discrte, Ph.D. thesis, Institut polytechnique de Grenoble, Grenoble, 2009. URL: `http://tel.archives-ouvertes.fr/docs/00/52/18/59/PDF/ThA_se_Luis_Olmos.pdf`.

[20] C. Kloss, C. Goniva, A. Hager, S. Amberger, S. Pirker, Models, algorithms and validation for opensource DEM and CFDDEM, Progress in Computational Fluid Dynamics, an International Journal 12 (2012) 140152.

[21] H. E. Exner, C. Mller, Particle rearrangement and pore space coarsening during solid-state sintering, Journal of the American Ceramic Society 92 (2009) 1384–1390.

[22] S. Martin, R. Parekh, M. Guessasma, J. Léchelle, J. Fortin, K. Saleh, Study of the sintering kinetics of bimodal powders. a parametric dem study, Powder Technology 270 (2015) 637–645.

[23] R. L. Coble, Effects of particle-size distribution in initial-stage sintering, Journal of the American Ceramic Society 56 (1973) 461–466.

[24] G. Wulff, Zur frage der geschwindigkeit des wachstums und der auflösung der kristallflächen, Z. kristallogr 34 (1901) 449–530.

[25] C. Krill III, L.-Q. Chen, Computer simulation of 3-d grain growth using a phase-field model, Acta Materialia 50 (2002) 3059–3075.

[26] J. Bruchon, F. Pino-Muoz, D.and Valdivieso, S. Drapier, Finite element simulation of mass transport during sintering of a granular packing. part i. surface and lattice diffusions, Journal of the American Ceramic Society 95 (2012) 2398–2405.

[27] K. Shinagawa, Simulation of grain growth and sintering process by combined phase-field/discrete-element method, Acta Materialia 66 (2014) 360 – 369.